# Numerical Simulations of Two-Stroke Cycle Engines Using Coal Fuels

**S. Kishan**
Engineering and Environmental Analysis Division, Radian Corporation, Austin, TX 78766

**S. R. Bell**

**J. A. Caton**

Department of Mechanical Engineering, Texas A&M University, College Station, TX 77843

*An analytical model of a two-stroke cycle, reciprocating, compression ignition engine was used to investigate the ignition and combustion characteristics of coal/water slurry fuels. The engine cycle simulation was based on a thermodynamic analysis of the cylinder contents and consisted of models for the injection, ignition, combustion, mixing, heat transfer, work, and scavenging processes. The thermodynamic analysis resulted in a set of first-order nonlinear, ordinary differential equations which were numerically integrated to obtain instantaneous cylinder gas, droplet, and particle conditions. The simulation results were first compared to experimental data from a large, slow-speed (120 rpm) engine using a coal/water slurry fuel. Complete validation of the model was not possible due to the lack of detailed experimental data, but comparisons are presented which indicate general agreement between measured and computed values. The model was then used to predict the performance of an engine representative of a locomotive medium-speed engine. Engine and fuel parameters were varied to study their effect on ignition and combustion of the coal/water slurry fuel and on the indicated engine performance. Increases in the inlet air temperature improved the ignition and combustion characteristics. Lower equivalence ratios or smaller particle sizes resulted in higher thermal efficiencies. Also, higher reactive coal led to increased cylinder pressures and higher thermal efficiencies due to faster burning rates.*

## Introduction

The need for developing alternative fuels for reciprocating, internal-combustion engines has been growing in recent years. This is primarily the result of the depletion of petroleum supplies and has led to the consideration of fueling engines with coal fuels. Interest in coal fuels is motivated by the economic and strategic advantages of coal relative to petroleum fuels [1, 2]. Applications of coal-slurry-fueled engines would be especially suited for low- and medium-speed engines since the difficult problems of fuel handling, wear prevention, and low burning rates are accentuated as engine speed increases. Specific applications which would be especially suitable for solid-fueled engines consist of stationary power plants, marine propulsion systems, and railroad locomotives. Many of these large engines are based on two-stroke cycle designs to provide favorable power-to-weight ratios.

Recent work has shown that reasonable success with coal fuels in reciprocating engines can be achieved. In some cases, performance of coal-fueled engines has been reported to be the same as that of oil-fueled engines [3]. Past work has identified several areas of concern, however, with the combustion of coal fuels in engines. In particular, the ignition of coal fuels in engines has been shown to be sensitive to the cylinder gas conditions [4, 5].

This investigation used a cycle simulation [6, 7] for two-stroke cycle engines which was developed for diesel or coal slurry fuel. The simulation was modified to include a more representative combustion process [8, 9] which will be described in a subsequent section. Two different engines were modeled: a very large, slow-speed (120 rpm) engine and a large, medium-speed (900 rpm) engine. The slow-speed engine was selected primarily because the only published experimental data of successful coal-fueled engine op eration were obtained from a Sulzer Brothers' 1 RSA 76 engine [3]. The medium-speed engine was selected since a major thrust for utilizing coal slurry fuels is for locomotive applications. One such two-stroke cycle, medium-speed engine is the General Motors' EMD 710 engine.

The specific objectives of this investigation were to develop simple models of the dominant processes, to integrate these models into a complete engine cycle simulation, and to use the simulation to explore the combustion and engine performance characteristics of the two engines using coal/water slurry fuel. Due to the lack of some experimental details, definitive validations of the cycle simulation were not possible, but comparisons are presented which indicate general agreement between measurements and computations.

## Model Description

An engine cycle simulation has been developed [6, 7] for a conventional open chamber, direct-injected, compression-

Contributed by the Internal Combustion Engine Division and presented at the Energy-Sources and Technology Conference and Exhibition, New Orleans, Louisiana, February 23–27, 1986. Manuscript received at ASME Headquarters April 30, 1986. Paper No. 86-ICE-13.

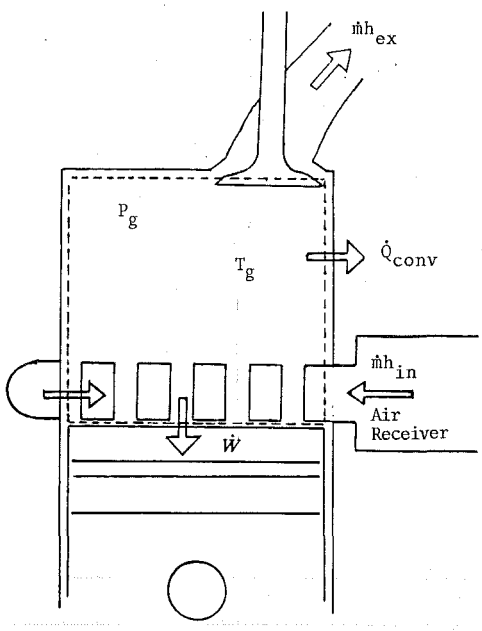


**Fig. 1 A schematic diagram of the engine piston and cylinder with the thermodynamic components denoted**

ignition, two-stroke cycle engine. The simulation was structured to model both loop- and uniflow-scavenged, two-stroke cycle engines. The simulation models the scavenging, compression, expansion, combustion, and exhaust processes of the two-stroke cycle. The various processes are modeled on the basis of a thermodynamic analysis of the cylinder gas by utilizing submodels for scavenging, wall heat transfer, intake, and exhaust processes and a detailed model for combustion. The original combustion model has been enhanced and now includes cylinder gas mixing as well as solid coal particle combustion, coal devolatilization, and liquid fuel evaporation and combustion.

To obtain the instantaneous cylinder gas thermodynamic state, the first law of thermodynamics was applied to the control volume illustrated in Fig. 1. The energy equation for the cylinder contents is

$$\frac{dE_g}{dt} = -\dot{W} + \sum_i \dot{Q}_i - \sum_j \dot{m}_j h_j \tag{1}$$

The cylinder contents were divided into individual regions and zones which are described below. Equation (1) is applied to each of the regions during scavenging, to each of the zones during combustion, and to all the cylinder contents during compression and expansion. The change in the gas energy may also be expressed in terms of internal energy as

$$\frac{dE_g}{dt} = m_g C_v \dot{T}_g + \dot{m}_g C_v T_g \tag{2}$$

From equations (1) and (2) an expression for the change in gas temperature is obtained as

$$\dot{T}_g = \frac{1}{m_g C_v}\left(-\dot{W} + \sum_i \dot{Q}_i - \sum_j \dot{m}_j h_j - \dot{m}_g C_v T_g\right) \tag{3}$$

This equation is then integrated for each region during scavenging and for each zone during combustion to yield the instantaneous local temperature. The next few paragraphs describe the submodels.

The scavenging model is based on the experimental work of Dedeoglu [10] and the analytical work of Benson [11], but was developed here for both uniflow- and loop-scavenged systems. The details of the overall scavenging model are described elsewhere [6, 7] and are only summarized here. The first part of scavenging was modeled as exhaust blowdown which occurred when the exhaust ports/valves opened and then proceeded in three phases while both the intake ports and exhaust ports/valves were open. The three scavenging phases are: a displacement phase, a mixing phase, and a short circuiting phase. Figure 2 is a schematic illustration of the exhaust blowdown, the three scavenging phases, and the regions used to model the scavenging process for a uniflow-scavenged process. The cylinder was divided into three regions: one for air, one for combusted gas, and one for mixed gas (air and combusted gas). The mixed gas region is determined by using a mixing ratio based on the incoming jet velocity, which specifies the amount of incoming air and combusted gas that form the mixed zone at each crank angle [6].

## Nomenclature

aTDC = after top dead center
aBDC = after bottom dead center
bTDC = before top dead center
bBDC = before bottom dead center
CA = crank angle
CIE = coal slurry injection end
CIS = coal slurry injection start
$C_v$ = constant volume specific heat of cylinder gas
$D$ = diameter
DIE = diesel injection end
DIS = diesel injection start
$E_g$ = internal energy of the cylinder gas
$E$ = activation energy
$F$ = pressure correction factor (see [13])
$h$ = enthalpy of cylinder gas
$k_{1,2}$ = reaction rate constant
$m$ = mass
$\dot{m}$ = time derivative of mass; mass flow rate
$P_g$ = cylinder gas pressure
$\dot{Q}_{comb}$ = heat release from combustion
$\dot{Q}_{conv}$ = convective heat transfer rate
$\dot{Q}_i$ = heat transfer or heat release from zone $i$
$\dot{Q}_{rad}$ = radiation heat transfer rate
$\dot{Q}_{sr}$ = heat release from surface reactions
$R$ = gas constant
$t$ = time
$T_g$ = temperature of cylinder gas
$T_{packet}$ = temperature of packet gas
$\dot{T}_g$ = time derivative of temperature
$V$ = instantaneous evolved volatile mass fraction
$V_{max}$ = maximum volatile yield
$\dot{W}$ = rate of piston work
$\alpha_{1,2}$ = rate constant multiplier
$\alpha_g$ = thermal diffusivity of gas
$\eta$ = engine thermal efficiency
$\theta_b$ = entrainment constant
$\rho$ = density
$\tau$ = ignition delay time parameter
$\phi$ = equivalence ratio

**Subscripts**

$a$ = air
$d$ = droplet
$ea$ = entrained air
$ex$ = exhaust
$g$ = gas
$i$ = heat transfer zone
$j$ = flow surface
$l$ = liquid
$p$ = particle
$s$ = solid
$v$ = volatiles

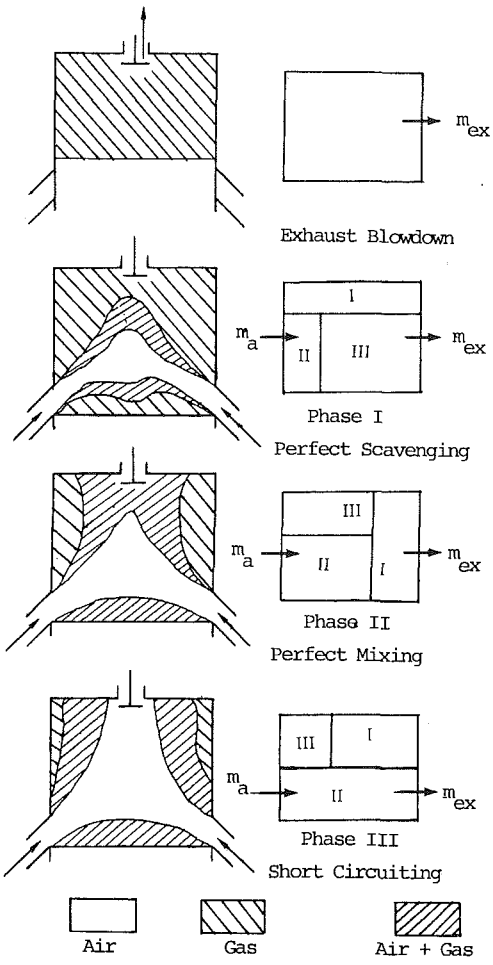


Fig. 2 A schematic of the scavenging model

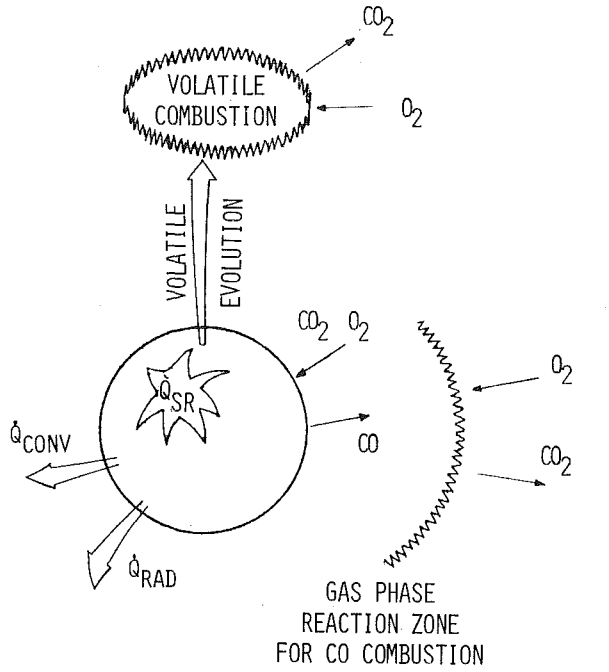


Fig. 3 A schematic of the components and processes for the combustion and devolatilization of a coal particle

Scavenging proceeds as the intake ports open and fresh air "jets" into the cylinder and displaces the combusted gas toward the exhaust valves/ports (the displacement phase). During this phase, the exhaust gas does not contain any fresh air and, hence, this phase is also called the perfect scavenging phase. In the second phase, a part of the mixture (fresh air and combusted gas), which formed during the first stage and which continues to form due to the presence of both fresh air and combusted gas in the cylinder, leaves the cylinder as exhaust gas. This is termed the perfect mixing phase. The third phase is the short-circuiting phase, which occurs when some of the incoming fresh air passes straight through to the exhaust ports/valves.

The combustion model was based on nonuniform mixtures within the cylinder due to fuel/air stratification. This was modeled by using multiple zones and the details of this model are given elsewhere [8, 9]. Each zone (not to be confused with the regions of the scavenging model) is formed by dividing the total fuel requirement into a number of packets as the fuel is injected. The mass of fuel in each packet is then divided into a number of fixed diameter droplets and particles. For most of this work, the slurry fuel was assumed to be atomized into droplets and coal particles with 30 and 10-$\mu$ diameters, respectively. Each packet is identified by a time of entry into the cylinder and by a classification scheme to permit different characteristics. Once injected, air from the "unburned zone" is entrained into each of the packets based on an entrainment function.

Fuel/air stratification is achieved by using an entrainment function which mixes different amounts of air into each of the packets. The entrainment function was formulated to include the major features of air entrainment while still remaining relatively simple. It was based on the fact that the entrained mass should be related to the mass of the unburned mixture and that during injection the entrained mass should increase as the jet develops. The entrained mass was also assumed to be a function of a packet's time of entry and classification. Such features were included in a simple exponential function [8, 9]. The entrained mass $m_{ea}$ is given by

$$m_{ea}(I, J) = \frac{m_{ub}}{I_t J_t}\left(\frac{\Delta\theta_{calc}}{\theta_b}\right)\exp\left[-\frac{I}{I_t}\frac{J}{J_t}\right] \tag{4}$$

where $I$ = index of packet entry into cylinder; $J$ = index of packet classification; $\theta_b$ = entrainment constant (°CA); $m_{ub}$ = instantaneous mass of unburned zone; $I_t$ = total number of packet entry times; $J_t$ = total number of packet classifications; $\Delta\theta_{calc}$ = calculation time step (°CA). Each packet is described by an entry index $I$ and a packet classification index $J$. The first packets injected into the cylinder have an index of 1; the second have an index of 2; and so forth. At each entry time the packets are also identified with a classification index (e.g., 1, 2 . . .).

The thermodynamic state of the gas in each of the zones is given by equation (3), where

$$\sum_i \dot{Q}_i = \dot{Q}_{comb} - \dot{Q}_{conv} \tag{5}$$

$$\sum_j \dot{m}_j h_j = \dot{m}_{ea} h_{ea} - \dot{m}_p h_p - \dot{m}_v h_v - \dot{m}_l h_l \tag{6}$$

The combustion term $\dot{Q}_{comb}$ is composed of three constituents which represent the energy release from the coal, volatiles, and liquid fuel vapor combustion. During injection, a charge of fuel mixture which is composed of specified amounts of liquid carrier and coal enters the cylinder. The coal consists of a specified mass fraction of char and volatiles. The particle combustion model is similar to the one developed by Caton and Rosegay [12] and modified to include devolatilization by Bell and Caton [13]. This model assumes spherical particles with uniform but time-varying temperatures. Also, this model includes variable particle

heating values and variable particle densities due to devolatilization. Figure 3 shows schematically the coal particle combustion process which includes solid phase reactions, gas phase reactions, and devolatilization. The particles are assumed to burn via two mechanisms yielding carbon monoxide

$$C_{(s)} + \frac{1}{2} O_{2(g)} \rightarrow CO_{(g)} \tag{7}$$

and

$$C_{(s)} + CO_{2(g)} \rightarrow 2CO_{(g)} \tag{8}$$

The carbon monoxide is then assumed to mix immediately with available oxygen in the packet and burn in the gas phase away from the particle. The standard surface kinetics was obtained from the literature as reported in [12, 14]. By simultaneously satisfying the mass conservation equations and surface kinetics of the particle, the reaction rates are calculated [12, 14].

A second constituent to the combustion term in the energy equation is from volatile combustion. A detailed description of the devolatilization model may be found elsewhere [13, 15] and, therefore, is only summarized here. Based on the assumption that the volatiles are locally released and jet away from the particle, a simple model was formulated for the devolatilization process. Once evolved, the volatiles are assumed to react with available oxygen in the packet (after an ignition delay) far from the particle. The assumption that the volatiles are locally released from the particle has been supported by several experimental observations [16–18]. If thermochemical conditions are sufficient, simultaneous solid particle reaction and devolatilization may occur. Since fundamental, mechanistic rate expressions for devolatilization are not available due to the complexities of the process, empirical data were used which have been approximated with first-order reactions such as

$$\frac{dV}{dt} = (\alpha_1 k_1 + \alpha_2 k_2) F (V_{max} - V) \tag{9}$$

where the rate constants $k_i$ are given by Arrhenius expressions. For the current study, the rate constants recommended by Kobayashi et al. [19] were used and 50 percent of the coal mass was assumed to be the maximum volatile yield.

A final constituent of the combustion term is the liquid fuel combustion. For simplicity, the steady-state, isolated, single drop approach of Spalding [20] was used. Vaporized fuel then mixes with available oxygen in the packet and reacts after an ignition delay.

The ignition delay correlation is used to determine the time between when the fuel is injected and the vaporized mixture ignites. (The correlation used here for the fuel vapor and volatiles should not be confused with the overall engine ignition delay times, which are based on the net effect of all the fuel on pressure recovery in the cylinder after injection.) The ignition delay correlation used in this study was that of Spadacinni and TeVelde [21] and is of the form

$$\tau = \frac{A}{P^n} \exp\left(\frac{E}{RT}\right) \tag{10}$$

where $A = 2.43 \times 10^{-9}$, $E = 41.56$ kcal/mole, and $n = 2$. This correlation has been used successfully in other cycle simulations [22].

Other terms in equation (3) such as piston work were calculated with a knowledge of the instantaneous cylinder conditions. The convective heat transfer includes convection from the particle and heat losses to the droplet and cylinder walls. The heat losses to the walls were calculated using an empirical correlation from Woschni [23] based on the average cylinder gas temperature. Heat transfer between the packets and the unburned zone was based on the volume (surface area) and temperature of the specific packet. Depending on the temperature of the packet this heat transfer may be to or from the packet. In addition to heat transfer across packet boundaries, packet work due to expansion or contraction is also transferred between packets. Droplet and particle convection rates were based on coefficients corresponding to droplets and particles in a quiescent atmosphere. Radiation losses from the particle to the cylinder wall were also included in the model.

**Table 1 Engine specifications**

| | Engine A* | Engine B† |
|---|---|---|
| Bore (*mm*) | 760 | 230.2 |
| Stroke (*mm*) | 1550 | 279.4 |
| Compression Ratio | 10.63 | 16 |
| Speed (rpm) | 120 | 900 |
| Normal Injection Timing (bTDC) | 6° | 15° |
| Inlet Air Temperature (K) | 350 | 310 |
| Air Receiver Pressure (kPa) | 240 | 260 |
| Exhaust Pressure (kPa) | 200 | 220 |
| Scavenging | Loop | Uniflow |
| Exhaust valve/port | Port | Valve |
| Number per Cylinder | 5 | 4 |
| Valve/Port open (bBDC) | 67° | 71° |
| Valve/Port close (aBDC) | 67° | 67° |
| Port Height (*mm*) | 217 | - |
| Port Breadth (*mm*) | 110 | - |
| Valve Diameter (*mm*) | - | 63.5 |
| Valve Max. Lift (*mm*) | - | 17.42 |
| Intake Ports | | |
| Number per Cylinder | 8 big/4 small | 18 |
| Height (*mm*) x Breadth (*mm*) | big : 180 x 55<br>small: 103 x 93 | 30 x 22 |
| Ports open (bBDC) | 45° | 43.5° |
| Ports close (aBDC) | 45° | 43.5° |

* Similar to the Sulzer Brothers' research engine 1 RSA 76.

† Similar to the General Motors' EMD710 engine.

**Table 2 Coal/water slurry fuel specification**

| | |
|---|---|
| % Liquid Carrier (by mass) | 50.0 |
| Maximum Volatile Yield ($V_{max}$) | 0.50 |
| % Volatile Matter (by mass) | 50.0 |
| Coal Heat of Combustion (kJ/kg) | 34,337 |
| Volatile Heat of Combustion (kJ/kg) | 35,000 |
| Char Heat of Combustion (kJ/kg) | 32,790 |

## Results

The purpose of this study was to use a cycle simulation for medium-speed locomotive engines to investigate engine operation using coal fuels. Further, the purpose of this work was also to conduct a sensitivity and parametric analysis of model variables, engine design parameters, and fuel properties. The only available experimental data for coal/water slurry fueled engines are for a slow-speed, large engine [3] (designated as engine A). The cycle simulation results were first compared to these experimental data. The model variables were varied to find the sensitivity of the computed results to their selection. These variables included the amount of pilot fuel, the coal particle size, the diesel droplet size, the surface and volatile reaction rates, the air receiver pressure, the entrainment constant, and the scavenging parameters. A detailed description

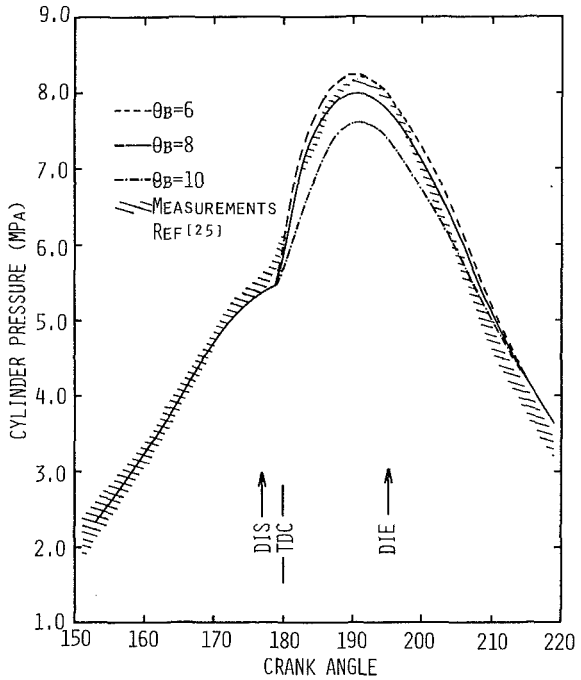


**Fig. 4 Cylinder gas pressure as a function of crank-angle for engine A using diesel fuel at 90 percent load for three entrainment constants**

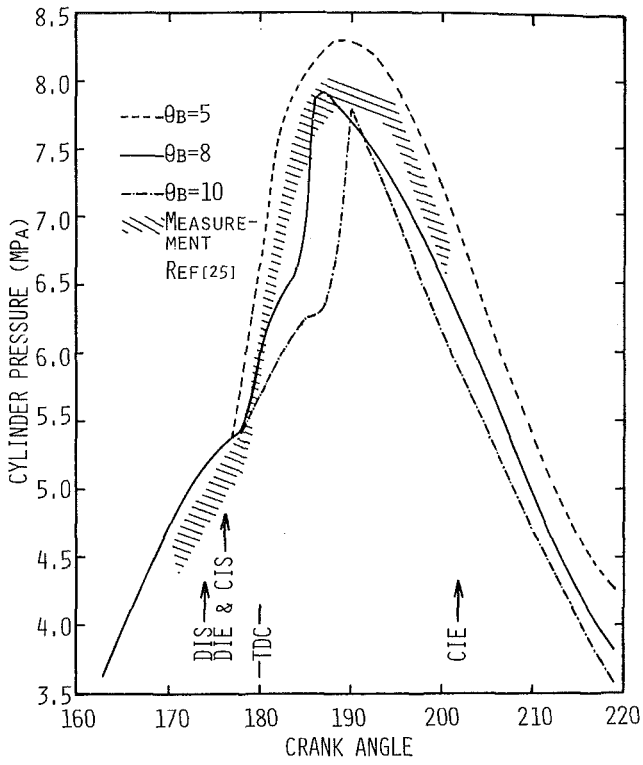


*Fig. 5 Cylinder gas pressure as a function of crank angle for engine A using coal/water slurry fuel at 90 percent load for three entrainment constants*

of the effect of all these variables on the results is given elsewhere [24]. In this paper, the effect of only a few of the significant variables on the computed results will be described.

Table 1 lists the specifications for the slow-speed engine, as well as for the medium-speed engine (designated as engine B). Table 2 lists the specifications of the coal slurry fuel. The results are for monosize particles and droplets with 10 and 30-$\mu$ diameters, respectively. The particles and droplets were assumed to be independently present in each of the packets and the liquid component was assumed not to cover the particles. Results for other particle/droplet arrangements have been presented by Bell and Caton [9]. For the cases they examined, they concluded that the specific arrangement did not significantly affect the results. The results section of this work is divided into two main sections, one for each engine.

**Engine A.** As very limited experimental data are available for coal slurry combustion in reciprocating engines, complete validation of coal-fueled engine simulations is not yet possible. The comparisons are limited to cylinder pressure as a function of crank angle. For engine A, the resutls that follow are first for the diesel fuel case and then for coal/water slurry fuel case. These results for engine A are for 90 percent load since the available experimental data [25] were for 90 percent load. Figures 4 and 5 (for diesel and coal/water slurry fuel, respectively) show the comparison of computed and measured cylinder pressures as a function of crank angle for engine A for three entrainment constants. The hatched regions on these figures represent estimates of the measured cylinder pressure from [25]. The cylinder pressure data presented in [25] did not include an absolute pressure scale. The actual cylinder pressures were scaled from the curves presented in [25] by knowing the peak firing pressure and the peak motoring pressure [26]. This procedure resulted in some uncertainties which are reflected by the hatched region.

Table 3 lists the comparison of the indicated performance parameters for engine A using diesel fuel. The indicated perforemance figures were compiled from [3, 25, 26] based on brake performance and an assumed 94.5 percent mechanical efficiency. The results in Fig. 4 and Table 3 indicate that the cycle simulation yields results which are in good agreement with the measurements. The specific set of model parameters

**Table 3 Engine A performance using diesel fuel (90 percent load)**

| Parameter | Computed | Measured |
|---|---|---|
| Indicated Power (kW/cyl) | 1390 | 1400* |
| Indicated MEP (kPa) | 989 | 995* |
| Indicated SFC (g/kW-hr) | 195 | 198* |
| $\eta_{indicated}$(%) | 42.8 | 43.3* |
| Air Flow Rate (kg/hr/cyl) | 13,172 | 13,760 |
| Fuel Flow Rate (kg/hr/cyl) | 272 | 272 |
| Maximum Pressure (MPa), at (aTDC) | 8.0, 10.1° | 8.2, 10° |

* Based on brake performance and 94.5% mechanical efficiency [3,25,26]

selected for these calculations, however, is not unique. The sensitivity of the results to the model parameters was examined [24] and the effects of major model variables on the results are described in the following paragraphs. As illustrated in Fig. 4, the selection of the entrainment constant $\theta_b$ affects the computed cylinder pressures in a modest manner. A lower entrainment constant $\theta_b$ causes a higher rate of air entrainment resulting in better combustion. As shown, an entrainment constant of 8 (the units of the entrainment constant are °CA, but these units will be omitted in the subsequent discussion for simplicity) resulted in cylinder pressures which agreed the best with the available data.

Figure 5 shows the comparison of computed and measured cylinder pressure for engine A using coal/water slurry fuel with a diesel fuel pilot. The pilot used was 17 percent of the total energy input [3] and was injected for 3°CA before the coal/water slurry was injected. The computed results for the coal slurry fuel case were based on the same power output as for diesel fuel (90 percent load). Data from [3, 25] were then used to compute the fuel input. Table 4 lists the computed performance parameters. The indicated performance figures were

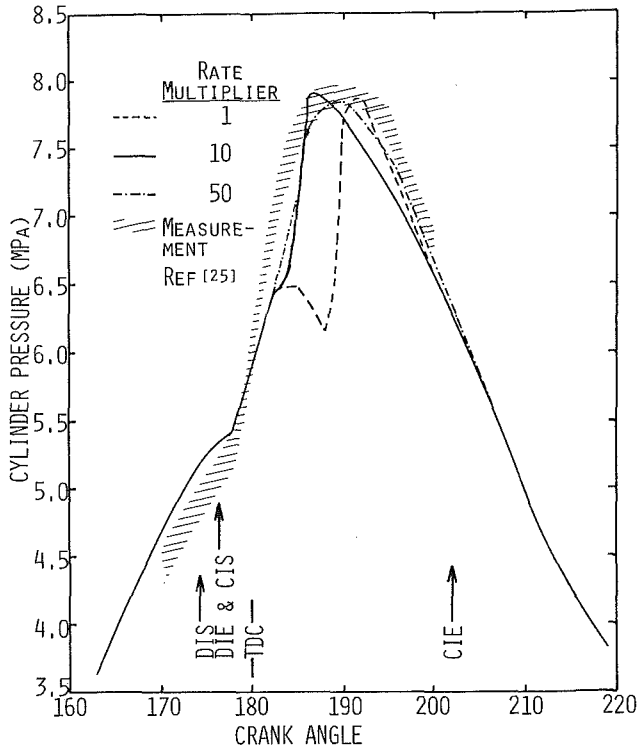


Fig. 6 Cylinder gas pressure as a function of crank angle for engine A using coal/water slurry fuel at 90 percent load for three pre-exponential reaction rate multipliers

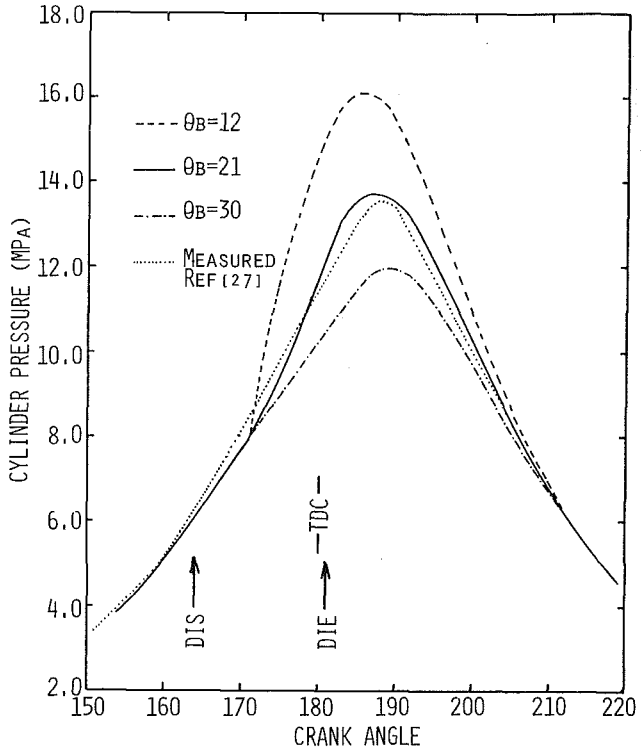


Fig. 7 Cylinder gas pressure as a function of crank angle for engine B using diesel fuel at 100 percent load for three entrainment constants

not available and, since the measured cylinder pressures [25] were only available for 80°CA near top dead center (TDC), no estimate of measured indicated engine performance could be inferred from the pressure measurements.

The computed performance was dependent on the selected model parameters and coal properties [24]. Figure 5 shows the variation of computed cylinder pressure for three values of the entrainment constant $\theta_b$. The pilot diesel fuel injected evaporates (due to the high gas temperatures) and is available to form combustible mixtures within the first few crank angles. The quantity of air in each of the packets, however, is limited by the entrainment process. Lower values of $\theta_b$ result in faster entrainment and better combustion for the diffusion limited reactions. As shown in Fig. 5, an entrainment constant of 8, as for the diesel case, yielded cylinder pressures which agreed with the measurements. The figure also shows that for engine A, a $\theta_b$ of 10 is very close to the critical value required for successful ignition. A comparison between the results of Figs. 4 and 5 indicates that for the operating conditions studied the combustion process was more sensitive to the amount of entrainment for the coal fuel than for the diesel fuel.

Figure 6 shows the sensitivity of the combustion process to the surface reaction rates and the devolatilization rates. These results provide information regarding the use of coals with higher reactivities. The figure shows the variation of the cylinder pressure for engine A using coal/water slurry fuel (Table 2) for three different kinds of coal. This was achieved by multiplying both the surface reaction and devolatilization rates by factors of 50, 10, and 1. For the lowest reactive coal (a multiplying factor of 1), the cylinder pressure trace has two peaks. The first peak results as the diesel pilot burns completely but, due to the low-reactivity coal, the particle surface temperatures are not high enough to promote active devolatilization or surface reactions, which results in a decrease in cylinder pressure. As the fuel particle continues to heat up, the coal particles finally ignite and this results in the second pressure peak. Increasing the reactivities by a factor of 10 improved the combustion characteristics but further increases in reaction rates did not have a significant effect on the ignition and combustion characteristics. All the base-case computations for engine A have used surface reaction and devolatilization rates increased by a factor of 10.

Table 4 Computed performance using coal slurry fuel (90 percent load, engine A)

| | |
|---|---|
| Indicated Power (kW) | 1425 |
| Indicated MEP (kPa) | 10.1 |
| Indicated SFC (g/kW-hr) | 607 |
| $\eta_{indicated}$(%) | 35.3 |
| Air Flow Rate (kg/hr) | 13,200 |
| Fuel Flow Rate (kg/hr) | 866 |
| Maximum Pressure (MPa), at (aTDC) | 7.9, 8° |

**Engine B.** No experimental data are available for coal/water slurry combustion in locomotive engines. For the purposes of this study, the engine simulation was first validated with experimental data for engine B using diesel fuel. Table 5 shows the comparison of the computed and measured performance parameters derived from [27]. Figure 7 shows the computed and measured cylinder pressures as a function of crank angle. The entrainment constant $\theta_b$ was varied from 12 to 30 to find the best match between the computed and experimental data. As mentioned earlier, a higher value of $\theta_b$ results in lower entrainment rates which yields richer packet equivalence ratios, lower burning rates and lower cylinder pressures. Figure 7 and Table 5 show that good agreement between computed and measured data was obtained for an entrainment constant of 21. The diesel fuel case was, therefore, used for verification purposes.

The next set of results are for coal/water slurry fuel (Table 2) in engine B. No pilot was used as in the engine A case. Instead, good ignition characteristics were obtained with preheated (450 K) inlet air. The effects of the degree of preheat

**Table 5 Engine B performance using diesel fuel**

| Parameter | Computed | Measured |
|---|---|---|
| Indicated Power (kW/cyl) | 209 | - |
| Indicated MEP (MPa) | 1.2 | - |
| Indicated SFC (g/kW-hr) | 178.6 | - |
| Air Flow Rate (kg/hr/cyl) | 1455 | 1449 |
| Fuel Flow Rate (kg/hr/cyl) | 37.3 | 36.1 |
| Maximum Pressure (MPa), at (aTDC) | 13.7, 7.3° | 13.3, 7.4° |

**Table 6 Engine B computed performance using coal-water slurry fuel**

| | |
|---|---|
| Indicated Power (kW) | 137.21 |
| Indicated MEP (kPa) | 786 |
| Indicated SFC (g/kW-hr) | 223.3 |
| $\eta_{indicated}$(%) | 47.6 |
| Maximum Pressure (MPa), at (aTDC) | 12.1, 9.7° |

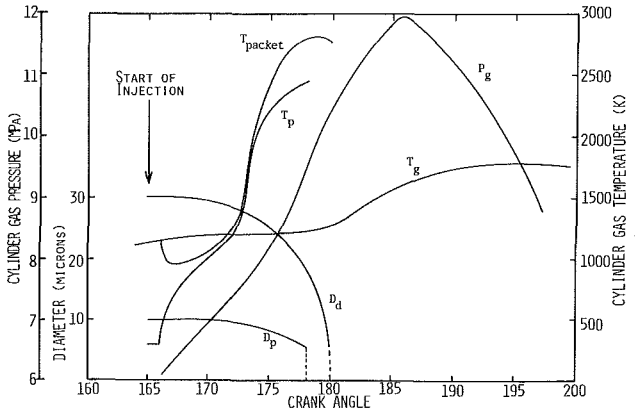


**Fig. 8 Results as a function of crank angle for a packet injected at the first crank angle of injection for engine B using coal/water slurry fuel**

on the ignition and combustion processes were also investigated [24]. Table 6 lists the performance results for this base case.

Figure 8 shows typical combustion results for engine B for the base case engine B as a function of crank angle. These results show the variation of packet, gas, and particle temperatures, particle and droplet diameters, and cylinder gas pressure and temperature for a packet injected at the first crank angle of injection and with a mid-classification. All packets behave in a similar fashion but have their own individual characteristics based on the crank angle of injection and their classification. The variation of cylinder gas pressure and temperature indicated the overall effect of all the individual packet burning on the cylinder gas. After injection, the liquid component of the slurry (water) immediately begins evaporating due to the high cylinder gas pressures and temperatures. The liquid evaporation causes a reduction in the local packet temperature, but this is only a short-term phenomenon. The coal particles start devolatilizing and, as the volatiles start burning (when the local equivalence ratios are lean enough), both the packet gas and particle temperatures increase. The increases in local gas temperatures further increase the particle temperature until significant devolatilization and coal combustion starts.

For all the parametric study results that follow, the injection timing was adjusted to obtain the best performance. The performance of the base case engine B was examined as a function of load (equivalence ratio) and particle sizes.

Figure 9 shows the indicated thermal efficiency as a function of equivalence ratio for engine B at a constant engine speed of 900 rpm. As the equivalence ratio is reduced from 1.0 to 0.3, the expected trend of increasing thermal efficiencies

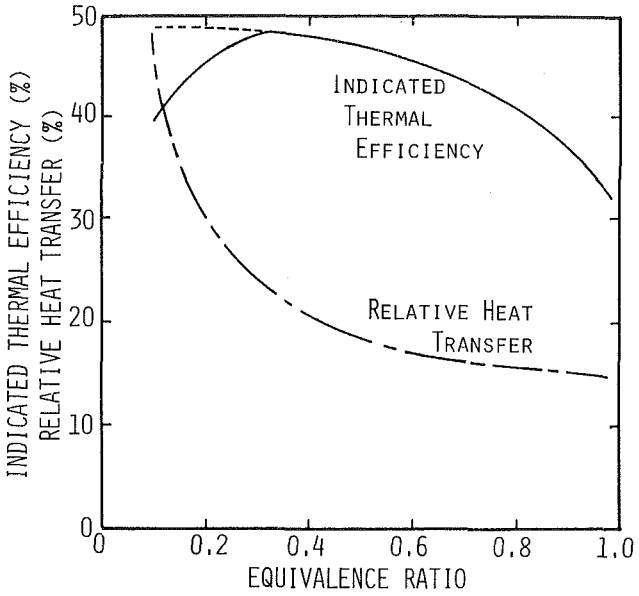


**Fig. 9 Indicated thermal efficiency and relative heat transfer as a function of equivalence ratio for engine B using coal/water slurry fuel**

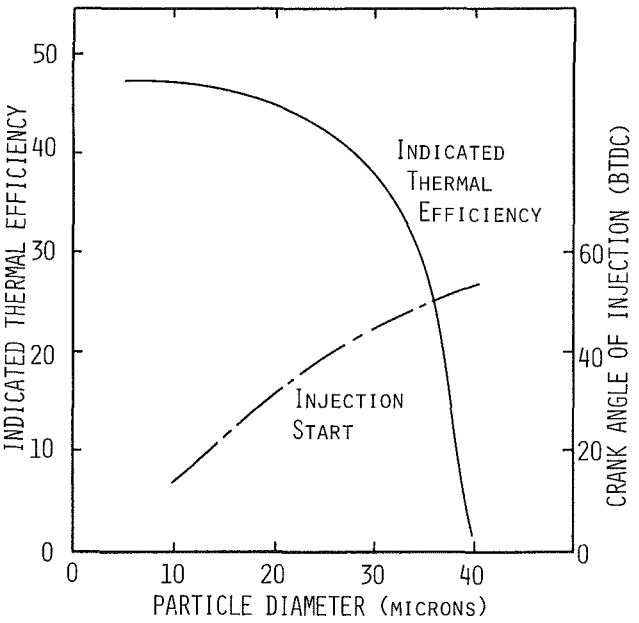


**Fig. 10 Indicated thermal efficiency and start of injection (for maximum efficiency) as a function of particle diameter of engine B using coal/water slurry**

was obtained due to the presence of excess air, improved burn times, and reduced absolute heat losses. As the equivalence ratio is reduced further, the indicated performance decreases for the case when injection duration is kept constant at 15° CA (solid line). These lower efficiencies are due to a small quantity of fuel injected over a relatively long injection duration leading to the heat release being spread over a longer crank angle duration. As the injection duration for the lower equivalence ratios is reduced (dashed line), in accordance with a lower rack setting at low loads, the small quantity of fuel is concentrated over a smaller injection duration and the heat release is closer to TDC leading to better performance as indicated by the dashed line in Fig. 9.

The lower curve in Fig. 9 shows the variation of relative heat transfer with equivalence ratio. Relative heat transfer is defined as the total heat transfer to the walls as a percentage of the total heat input. The curve is seen to increase sharply at

lower equivalence ratios mainly due to decreasing values of heat input. At lower equivalence ratios, the cylinder gas temperatures do not decrease much; therefore, the total wall heat transfer does not change substantially. The heat input decreases significantly, however, causing relative heat transfer to increase sharply.

Figure 10 shows the indicated thermal efficiency as a function of particle size for engine B. At a constant equivalence ratio, increasing the particle diameter resulted in fewer number of particles per packet. The larger particles had a smaller overall surface area available for surface reactions. This resulted in lower reaction rates, since energy is released over a greater crank angle duration, and lower indicated efficiencies. The lower plot in the figure shows the injection timing in crank angle degrees bTDC for best performance. Advanced injection timings are required for the large particles to compensate for the longer burn times.

## Summary and Conclusions

An engine cycle simulation was used which was based on a thermodynamic analysis with detailed combustion submodels to investigate the behavior of coal/water slurry combustion in large, two-stroke cycle engines. In brief, conclusions of this study include:

1 The combustion model developed in this work included a parameter, the entrainment constant, to model the process of air entrainment. An evaluation of this entrainment constant, as well as other model parameters and fuel properties was completed to establish the sensitivity of the cycle simulation to these parameters. For a specific set of model parameters and coal properties, computed engine characteristics indicated good agreement with limited available measurements.

2 Higher air entrainment rates resulted in better performance characteristics, which indicates that the combustion process is largely a diffusion or mixing-controlled process.

3 Coal fuels with higher reactivities exhibited better ignition characteristics, and yielded higher indicated efficiencies for the specific injection timings due to faster burning rates.

4 The engine inlet air temperature was an important parameter which controlled the ignition characteristics of coal/water slurry. Increasing the inlet air temperature resulted in better ignition characteristics.

5 Coal/water slurry fuel with smaller particle sizes exhibited higher indicated thermal efficiencies. At the same inlet air temperature, 40-$\mu$ particles did not ignite but 10-$\mu$ particles resulted in a 48 percent indicated thermal efficiency.

## Acknowledgments

This work was supported by the U.S. Department of Energy, Morgantown Energy Technology Center, Contract No. DE-AC21-84MC21175, and by the Center for Energy and Mineral Resources, Texas A&M University.

## References

1 Caton, J. A., and Rosegay, K. H., "A Review and Comparison of Reciprocating Engine Operation Using Solid Fuels," SAE Paper No. 831362, 1983.

2 Carpenter, L. K., and Crouse, F. W., Jr., "Coal-Fueled Diesels, Fossil Energy Activities," ASME Paper No. 85-DGP-18, 1985.

3 Nydick, S. S., "Coal/Water Slurry Fueled Slow-Speed Diesel Engine Program: Past, Present and Future," Thermo Electron Corporation, MA, presented at "Coal-Fueled Diesel for Cogeneration Seminar," Rosemont, IL, July 25, 1985, Report No. TE4319-123-85.

4 Robben, F., Brehob, D. D., Namazian, M., Sawyer, R. F., and Sherman, P., "Coal Fueled Diesel Engines," *Proceedings of the Sixth International Symposium on Coal Slurry Combustion and Technology*, Orlando, FL, June 25–27, 1984.

5 Siebers, D. L., and Dyer, T. M., "The Autoignition and Combustion of Coal-Water Slurry Under Simulated Diesel Engine Conditions," ASME Paper No. 85-DGP-15, 1985.

6 Kishan, S., "Simulation Study of Two-Stroke Cycle Compression Ignition Engines," M.S. Thesis, Texas A&M University, May 1985.

7 Kishan, S., and Caton, J. A., "Simulation of a Two-Stroke Cycle, Locomotive Engine Using Diesel or Coal Fuels," presented at the Spring Central States Meeting of the Combustion Institute, San Antonio, TX, Apr. 22–23, 1985, Paper No. 1-1A.

8 Bell, S. R., and Caton, J. A., "Ignition and Combustion Characteristics of Coal Fuels in Diesel Engines," Report No. CF-85-01, Texas A&M University, Sept. 1985.

9 Bell, S. R., and Caton, J. A., "Analytical Evaluations of Ignition Options for a Coal/Water Slurry Fueled Engine," presented at the Fall Meeting of the American Flame Research Committee, Livermore, California, Oct. 17–18, 1985.

10 Dedeoglu, N., "Scavenging Solves Problems in Gas Burning Engines," SAE Paper No. 710579, 1971.

11 Benson, R. S., "A New Gas Dynamic Model for the Gas Exchange Process in a Two-Stroke Loop and Cross Scavenged Engines," *Inst. J. Mech. Sci.*, Vol. 19, 1977, pp. 693–710.

12 Caton, J. A., and Rosegay, K. H., "An Analysis of Solid Particle Combustion in an I.C. Engine Environment," presented at the Central States Section Meeting of the Combustion Institute, Lexington, KY, Mar. 21–22, 1983, Paper No. CSS/CI 83-02.

13 Bell, S. R., and Caton J. A., "Cycle Simulations for a Reciprocating, Internal Combustion Engine Using a Coal Slurry Fuel: the Role of Volatiles," presented at the American Flame Research Committee International Symposium on Alternate Fuels and Hazardous Wastes, Tulsa, OK, Oct. 9–11, 1984, Paper No. 4.1.

14 Rosegay, K. H., and Caton, J. A., "Cycle Simulation of Coal Particle Fueled Reciprocating Internal Combustion Engine," SAE Paper No. 831299, 1983.

15 Bell, S. R., and Caton, J. A., "Cycle Simulations for a Reciprocating, Internal Combustion Engine Using a Coal Slurry Fuels," presented at the Spring Central States Meeting of the Combustion Institute, San Antonio, TX, Apr. 22–23, 1985, Paper No. 2-1A.

16 Mathews, K. J., and Street, P. J., "Combustion Histories of Various Coal-Water Fuels," presented at the Sixth International Symposium on Coal Slurry Combustion and Technology, Orlando, FL, June 25–27, 1984.

17 Seeker, W. R., Samuelson, G. S., Heap, M. P., and Trolinger, J. D., "The Thermal Decomposition of Pulverized Coal Particles," *Eighteenth Symposium (International) on Combustion*, 1981, p. 1213.

18 McLean, W. J., Hardestey, D. R., and Pohl, J. H., "Direct Observations of Pulverized Coal in a Combustion Environment," presented at the Central States Section Meeting of the Combustion Institute, Baton Rouge, LA, Mar. 24–25, 1980, Paper No. CSS/CI 80-11.

19 Kobayashi, H., Howard, J. B., and Sarofin, A. F., "Coal Devolatilization at High Temperatures," *Sixteenth Symposium (International) on Combustion*, 1977, p. 411.

20 Spalding, D. B., *Some Fundamentals of Combustion*, Academic Press, London, 1955.

21 Spadacinni, L. J., and TeVelde, J. A., "Autoignition Characteristics of Aircraft-Type Fuels," *Combustion and Flame*, 1982, p. 46.

22 Mansouri, S. H., Heywood, J. B., and Radhakrishnan, K., "Divided Chamber Diesel Engine, Part I: A Cycle Simulation Which Predicts Performance and Emissions," SAE Paper No. 820273, 1982.

23 Woschni, G., "A Universally Applicable Equation for the Instantaneous Heat Transfer Coefficient in Internal Combustion Engines," SAE Paper No. 670937, 1967.

24 Kishan, S., Bell, S. R., and Caton, J. A., "Two-Stroke Cycle Engine Simulations: a Sensitivity Study," Report No. CF-85-04, Texas A&M University, Dec. 1985.

25 Steiger, H. A., "Sulzer Single Cylinder Test Results With Various Coal Water Slurries," presented at "Coal-Fueled Diesel for Cogeneration Seminar," Rosemont, IL, July 25, 1985.

26 Dunlay, J. B., Davis, J. P., Maslen, P. L., Stieger, H. A., and Eberie, M. K., "Economic and Technological Assessment of Diesel Engines Using Coal-Based Fuels for Electric Power Generation," Report No. TE4234-37-80, Thermo Electron Corporation, MA, Sept. 1979.

27 Kotlin, J. J., Dunteman, N. R., Chen, J., and Heilenbach, J. W., "The General Motors EMD Model 710G Series Turbocharged Two-Stroke Cycle Diesel Engine," ASME Paper No. 85-DGP-24-1985.